Pose Estimation with Unknown Focal Length using Points, Directions and Lines

Yubin Kuang, Kalle Åström
Centre for Mathematical Sciences
Lund University
{yubin,kalle}@maths.lth.se

Abstract

In this paper, we study the geometry problems of estimating camera pose with unknown focal length using combination of geometric primitives. We consider points, lines and also rich features such as quivers, i.e. points with one or more directions. We formulate the problems as polynomial systems where the constraints for different primitives are handled in a unified way. We develop efficient polynomial solvers for each of the derived cases with different combinations of primitives. The availability of these solvers enables robust pose estimation with unknown focal length for wider classes of features. Such rich features allow for fewer feature correspondences and generate larger inlier sets with higher probability. We demonstrate in synthetic experiments that our solvers are fast and numerically stable. For real images, we show that our solvers can be used in RANSAC loops to provide good initial solutions.

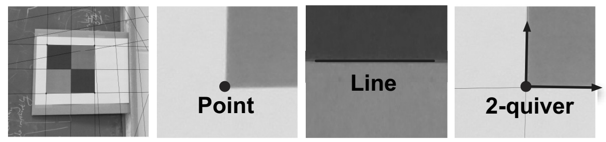

Figure 1. The figure illustrates three examples of image features in an image, a point with 2 degrees of freedom, a line with 2 degrees of freedom and a 2-quiver with 4 degrees of freedom. The 2-quiver consists of a point and two directions out from the point.

1. Introduction

The problem of camera pose estimation has been studied extensively in the computer vision community. The minimal case of pose estimation using 3 points was studied in [10] and several other formulations are compared and reviewed in [12]. For line-to-line correspondences, solutions are derived for minimal of 3 lines in [8, 7]. Recently, the minimal cases using combination of points and lines are solved in [27]. In [9] a solver is derived for a minimal problem of 2 points and their corresponding tangent directions (equivalently any direction vector through each of the points). The required correspondence is reduce to a single local patch correspondence in [20] . However, this specific setting is unfortunately very sensitive to measurement noise of the patches.

For camera pose estimation with unknown focal length, the planar case was studied and solved in [1]. For general non-planar cases, the close to minimal case using 4 2D-3D correspondences was first studied in [28]. Efficient and numerically stable solvers are developed in [4]. By combining 2D-2D and 2D-3D correspondence, [19] investigated several minimal cases for pose estimation with unknown focal length. Additionally, for camera with unknown radial distortion and unknown focal length, the 4-point minimal case is solved in [18, 5].

Many other works focus on solving the over-constrained problem of estimating camera pose with more than three points [15, 25, 24] or lines [25]. Very recently, the approach in [24] was extended to handle unknown focal length [26]. All of these method are based on formulation that minimizes certain algebraic errors and generally assume that there exist no outliers in the data. Minimal solvers are the key component of the preprocessing steps for such over-constrained solvers to robustly remove outliers.

To be able to utilize correspondences of geometric primitives like points, directions and lines is of great interest to applications e.g. structure and motion [17] and vision-based localization [16]. In this paper, we focus on the camera pose estimation problem given 2D-3D correspondence of such rich features. In typical scenarios of vision-based localization, focal length of the camera is the only unknown that is most difficult to determine accurately (EXIF-tag could provide erroneous estimate) and can render large errors in the pose estimation. All previous methods for pose estimation with unknown focal length use point correspondences. The contribution of this paper is to enable a wider class of geometric features (combinations of points, lines and n-quivers, Figure 1) for simultaneous pose estimation and focal length calibration. We show a straightforward but unified way to formulate polynomial systems for different combinations of

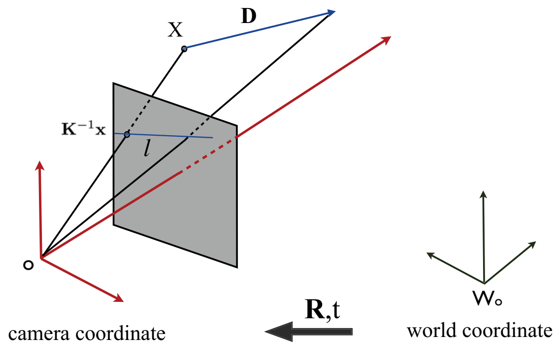

Figure 2. Camera coordinate, world coordinate, and the geometric relations of 2D-3D correspondences of point, line and direction.

features. We then develop efficient polynomial solvers for several new minimal cases and a slightly over-determined cases using 4 lines. We verify our solvers on both synthetic and real images to demonstrate their efficiency and usability in RANSAC.

2. Problem Formulation

In this paper, the standard pinhole camera model is used. For a 3D point $\mathbf{X}$ and it corresponding 2D image projection $\mathbf{x}$, the projection equation is,

$$\lambda \mathbf{x} = \mathbf{P}\mathbf{X}. \tag{1}$$

Here, $\mathbf{P}$ is the camera matrix of size 3×4 which can be factorized as,

$$\mathbf{P} = \mathbf{K}[\mathbf{R}|\mathbf{t}]. \tag{2}$$

The rotation matrix $\mathbf{R}$ encodes orientational part of the camera pose specifying in which direction the camera is pointing and $\mathbf{t}$ relates to the camera position. $\mathbf{K}$ is the calibration matrix of the camera and compensates for the intrinsic setup of the camera. For both practical camera setups and numerical stability, it is generally assumed that the cameras have centered principle points, square pixels with zero skew. In this paper, we thereafter assume that the calibration matrix only involves the unknown focal length f. The K matrix can be equivalently written as

$$\mathbf{K} = \begin{bmatrix} 1 & 0 & 0 \\ 0 & 1 & 0 \\ 0 & 0 & w \end{bmatrix}, \tag{3}$$

where $w = 1/f$ and f is focal length of the camera. We know that the problem of determining camera pose with unknown focal length has in total 7 degrees of freedom (3 in rotation, 3 in translation and 1 in f).

2.1. Number of Constraints

In this section, we discuss in details the constraints given by different geometric primitives.

Point Constraints: Given a known 3D point $\mathbf{X}$ and its corresponding image point $\mathbf{x} = \begin{bmatrix} u & v & 1 \end{bmatrix}^T$, it is well known that there are two constraints on $\mathbf{P}$ [14]. The two constraints can be chosen from the three linearly dependent equations based on (1) :

$$[\mathbf{x}]_\times \mathbf{P}\mathbf{X} = 0, \tag{4}$$

where

$$[\mathbf{x}]_\times = \begin{bmatrix} 0 & -1 & v \\ u & 0 & -1 \\ -v & u & 0 \end{bmatrix}.$$

Line Constraints: Given a known 3D line L and its corresponding image line $\mathbf{l}$, there are also two constraints on $\mathbf{P}$. If the 3D line L is represented as a 3D point $\mathbf{X}$ and the direction of the line $\mathbf{D}$, one can obtain two equations for the two points in the following form based on (1):

$$\begin{aligned} &\mathbf{l}^T\mathbf{P}\mathbf{X} = 0 \\ &\mathbf{l}^T\mathbf{P}(\mathbf{X} + k\mathbf{D}) = 0, \end{aligned} \tag{5}$$

where k is an arbitrary constant.

Quiver Constraints: For a known 3D point $\mathbf{X}$ and a directional measurement $\mathbf{D}$ through $\mathbf{X}$, given the corresponding image projection $\mathbf{x}$ and $\mathbf{d}$, there are three constraints on $\mathbf{P}$. We hereafter call the geometric primitive with a point and n directions passing through it as an *n-quiver*. First, we obtain two constraints from the point correspondence according to (4). The other constraint comes from the directional measurement. To see this, we first convert the measurement $\mathbf{d}$ along with $\mathbf{x}$ to a line measurement $\mathbf{l}$. Then we utilize the equations in the form of (5) and take the difference between them. Equivalently, we have

$$\mathbf{l}^T\mathbf{P}\mathbf{D} \quad = 0 \tag{6}$$

For a 2-quiver, we have in total four constraints including two point constraints and two constraints in the form of (6).

The number of constraints for different primitives are summarized in Table 1.

Point	Line	1-Quiver	2-Quiver
2	2	3	4

Table 1. Number of constraints enforced by 2D-3D correspondences of different geometric primitive for camera pose estimation.

2.2. Useful Cases

With 2D-3D correspondences of points, lines and n-quivers, one can form several novel minimal cases by searching for combination such that $2m_p + 2m_l + (n+2)m_q = 7$, where m_p, m_l, m_q are the number of point, line, n-quiver correspondences, respectively. We present and solve several of such minimal cases and also study a slightly over-determined cases using 4 lines.

Two Points and One 1-Quiver ($P2Q1$) : Given three points and one direction passing through one of the points, we can form 6 equations based on (4) and 1 equation based on (6). Thus this problem is minimal.

One 1-Quiver and One 2-Quiver ($Q1Q2$) : For two points, where one line passing through one of the point, and two lines passing through the other point are known, we can form 4 point equations (4) and 3 equations with respect to the directions (6). This yields also a minimal problem.

Four Lines ($P4L$) : Given 4 3D-2D line correspondences, there are in general 8 independent constraints. Thus, the problem of camera pose with unknown focal length is over-determined with 4 lines. We can choose 7 from the 8 equations, and use the eighth equation to verify a unique solution.

In a similar manner, other minimal cases include the setups: (i) one point, one line and one 1-quiver (ii) one 3-quiver and one point (iii) two lines and one 1-quiver which can be solved in similar manner as the presented solvers.

2.3. Parameterization

There exist many ways to parameterize the problems related to camera pose estimation. In [28], Triggs first parameterizes the camera as an arbitrary matrix with 12 unknowns, the solutions then lie in the null space of the linear constraints given by the point constraints. Then the quadratic constraints (orthogonality and equal norm) on the rotational part of the camera matrix is enforced afterwards. The benefits of this formulation is that one needs to only solve quadratic polynomial systems. Once the rotational part is recovered, the focal length can easily be calculated using the ratios between the norms of the third and the first two rows of $\mathbf{R}$. The drawback of this formulation is that non-planar and planar scenes need to be handled separately and explicitly as shown also in [5].

On the other hand, Bujnak et al. [4] formulate the P4P problem with unknown focal length using the invariance of the ratios of distances between the 3D points under rigid transformation. For directional correspondences, one can similarly make use of the invariance of the angles between the directions [9]. Here, we discuss briefly the application of such geometric invariance to the $P2Q1$ problem i.e. two points ($\mathbf{X}_1, \mathbf{X}_2$) and one point ($\mathbf{X}_3$) with a known direction ($\mathbf{D}$). To start with, we can use the three points to form 2 independent distance ratio equations involving three unknowns (two relative stretch ratios α_1,α_2 and f) as in [4]. Then for the known direction, one can form equations using the invariance of angles for $(\mathbf{D}, \mathbf{X}_3 - \mathbf{X}_1)$ and $(\mathbf{D}, \mathbf{X}_3 - \mathbf{X}_2)$. This again produces two independent equations involving all 4 unknowns (α_1, α_2, α_3, f). Thus, we obtain 4 equations with 4 unknowns. However, the resulting equations consists at least one equation of degree 6 (after substitution and simplification) which makes the resulting polynomial system very difficult to solve. While the use of geometric invariance might yield polynomial system with fewer solutions for previous problems, it is not straightforward to see that such property is preserved for other primitives like directions with unknown focal length.

In this paper, we first parameterize the rotation matrix $\mathbf{R}$ with quaternion and construct equations directly based on (4), (5) and (6). It turns out that this straightforward parameterization, produces polynomial systems that are relatively easy to solve and also general for both planar and non-planar scenes. In the rest of paper, the rotation matrix $\mathbf{R}$ is parameterized with quaternion according to

$$\begin{bmatrix} a^2+b^2-c^2-d^2 & 2bc-2ad & 2ac+2bd \\ 2ad+2bc & a^2-b^2+c^2-d^2 & 2cd-2ab \\ 2bd-2ac & 2ab+2cd & a^2-b^2-c^2+d^2 \end{bmatrix}. \quad (7)$$

To fix the scale of the quaternion, we set $a = 1$. Note that by setting $a = 1$, we reduce the number of unknowns which facilitates the polynomial system solving. This will in general introduces for degenerated rotations ($a = 0$) or potential numerical instability ($a \approx 0$). Due to the rare occurrences of such configuration, we will demonstrate in the experimental section such degeneracy does not affect the practical usage of the solvers.

From the factorization in (2), we know that $\mathbf{P}$ can be rewritten as:

$$\begin{bmatrix} a^2+b^2-c^2-d^2 & 2bc-2ad & 2ac+2bd & t_x \\ 2ad+2bc & a^2-b^2+c^2-d^2 & 2cd-2ab & t_y \\ w(2bd-2ac) & w(2ab+2cd) & w(a^2-b^2-c^2+d^2) & wt_z \end{bmatrix}.$$

where $\mathbf{t} = [t_x \ \ t_y \ \ t_z]^T$. If we additionally set $t'_z = wt_z$, we have in total 7 unknowns $\{b, c, d, t_x, t_y, t'_z, w\}$. Given different geometric primitives, the constraints (4), (5) and (6) are linear to $\{t_x, t_y, t'_z\}$. Thus, we can conveniently eliminate all three of them and rewrite the equations with respect to the 4 unknowns $\{b, c, d, w\}$ only. Specifically, for all the useful cases presented in Section 2.2, we can choose 3 of the equations to eliminate $\{t_x, t_y, t'_z\}$ and obtain 4 cubic equations with 4 unknowns (for $P4L$, there are 5 such cubic equations). In the next section, we will discuss the solutions to such polynomial systems.

3. Polynomial Solvers

To solve the polynomial systems in Section 2, we utilize the techniques developed based on Gröbner basis. Instead of using the automatic solver generator [22], we choose to use the techniques in [6] for better numerical stability. For polynomial systems with small number of unknowns, Gröbner basis methods are generally fast and numerically stable. Solving polynomial systems can also be seen as solving polynomial eigenvalue problems [13, 23]. We leave this as our future work.

We start by verifying the number of solutions. For instance, for minimal problem of two points and one 1-quiver ($P2Q1$), we verify using algebraic geometry tools Macaulay2 [11] in $\mathbb{Z}_p$ that there are in general 20 solutions. Recall from Section 2.3 that, after linear elimination, we are left with 4 equations with 4 unknowns $\{b, c, d, w\}$. To solve the polynomial system using the techniques in [6], we first multiply the 4 equations with all the monomials of total degree up to 6 and maximum degree of each variable as $[2, 2, 2, 3]$, respectively. In this way, we obtain an elimination template of 372 equations and 386 monomials. To enhance numerical stability, we employ the basis selection technique by choosing the permissible set (see more details in [6]) to be the last 35 monomials in *grevlex* ordering. After the QR factorization with column pivoting, we can construct the so-called *action matrix* of size 20×20 from which the solutions can be obtained by eigenvalue decomposition. After we solve for $\{b, c, d, w\}$, we can calculate the values of other unknowns using linear substitution.

For all the other cases, we find that the number of solutions is also 20 and the same elimination template gives very similar numerical stability. This could be due to the similar structures in the constraints of these problems.

4. Experiments

In this section, we study the performance of our solvers on both synthetic and real data.

4.1. Synthetic Data

For the synthetic experiments, we choose the size of image to be 1024×800. Random scenes were generated by drawing points uniformly from a cube with side length 800 centered at the origin. Then the directions through points were chosen randomly (either in planar or in non-planar fashion). A camera was placed at a distance of around 1000 from the origin, pointing approximately at the center. The camera was calibrated except for the focal length.

4.1.1 Stability and Number of Solutions

We evaluate first the solvers on noise-free data to check the numerical stability of the solvers and distribution of number of valid solutions. For the simulation results in Figure 3, the focal length of the camera was set to around 1000. The numerical errors for all our solvers are fairly low for most of the cases. We also note that the focal length is coupled i.e. if

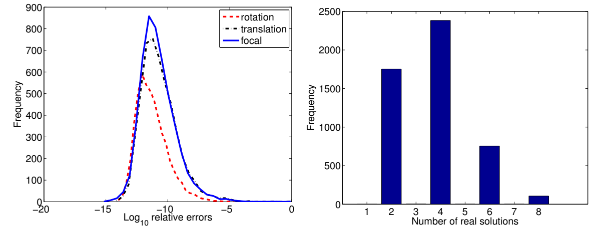

Figure 3. Two point and one 1-quiver, synthetic experiments for 5000 runs on noise-free data with focal length approximately 1000. **Left**: Histogram of relative errors for rotation, translation, focal length; **Right**: Histogram of number solutions with real and positive focal lengths.

f is solution, so is -f which corresponds to equivalent pairs of camera matrices $\mathbf{P}$ and $-\mathbf{P}$. This symmetry is caused by the quaternion parameterization. Since only the real and positive f are geometrically valid, one can safely remove the other solutions. In the simulation, it is shown that there are up to maximumly 8 solutions with real and positive f while most often only 2 or 4 solutions.

The boxplot in Figure 4 shows the medians, 25 percentiles and 75 percentiles of the distribution of the relative errors. We can see that for noise-free data, the Gröbner basis solver for ($P2Q1$) is consistently stable for different focal lengths for both planar and non-planar scenes (Figure 4). Similar numerical behaviors are observed for the solver using lines ($P4L$, Figure 5). Given that the performance of other solvers are similar, related figures are not shown individually here.

The solvers implemented in MATLAB takes approximately $15ms$. The computation is dominated by the first elimination using QR factorization. For comparison, the optimized $P4P$ solver in [4] runs at around $2ms$. Our solvers can also be further optimized for speed using strategies in [22, 21]. The time performance is measured on a Macbook Air with 1.8 GHz Intel Core i5 and 8 GB memory.

4.1.2 Noise Sensitivity

To study the behaviors of the solvers with noisy measurements, we add noise of different levels both to the image point positions and the angles of the directions. In Figure 6, it is shown that the $P2Q1$ solver gives fairly good estimates for focal lengths with small noise, and is still able to provide (though not as frequently) reasonably good initial solutions when the noise is around 5 pixels. We have also noticed that the solvers can be sensitive to errors in the direction measurements. We also test the $P4L$ solvers for noisy line measurements by perturbing the intersections between the lines and the x, y axis. From Figure 7, we can see that the $P4L$ solver is capable of recovering the focal length accurately for small perturbation and can become unreliable for large perturbation. To further understand the noise sensitiv-

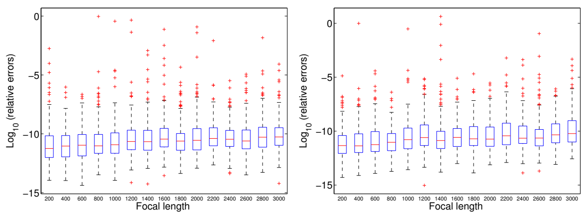

Figure 4. Synthetic experiments of $P2Q1$ on noise-free data with varying focal lengths. **Left**: Boxplot of relative errors of focal lengths for non-planar points and directions; **Right**: planar cases.

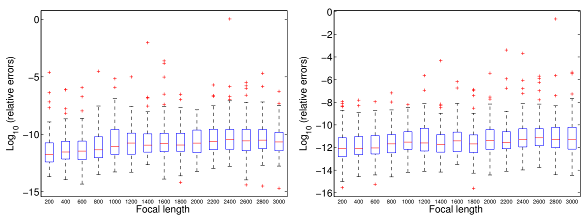

Figure 5. Synthetic experiment of $P4L$ on noise-free data with varying focal lengths. **Left**: Boxplot of the relative errors of focal lengths for non-planar line configurations **Right**: planar cases.

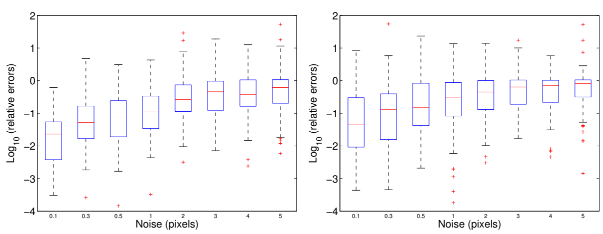

Figure 6. Synthetic experiments for $P2Q1$ on noisy data with varying noise levels on image point positions with fixed $f = 1000$ and angle perturbation of degree $[-0.1, 0.1]$. **Left**: Relative errors of focal lengths for non-planar points and directions; **Right**: planar cases.

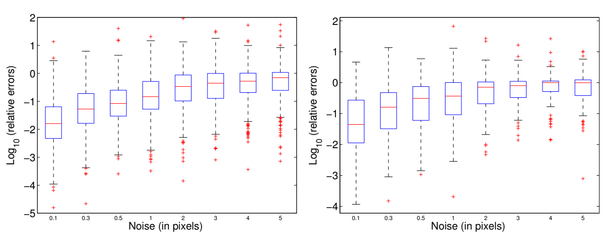

Figure 7. Synthetic experiments for $P4L$ with varying noise on the intersection points of between the lines and x, y axes with fixed $f = 1000$. **Left**: Relative errors of focal lengths for non-planar lines; **Right**: planar cases.

ity, we demonstrate the performance of the solvers on real image measurements in Section 4.2.

4.1.3 RANSAC Experiments

To test the advantage of the proposed solvers for different geometric primitives, we simulate data with outliers and

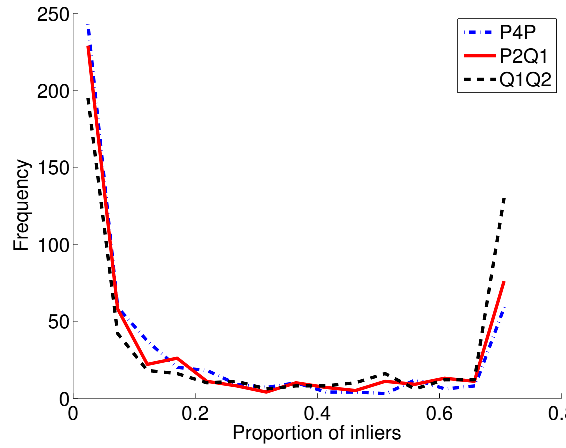

Figure 8. Distribution of inlier proportions for 1000 RANSAC runs for different solvers $P4P$, $P2Q1$ and $Q1Q2$.

RANSAC is used to obtain robust initial solution. For a fixed camera with focal length 1000, we generate randomly 1000 scene points as in the previous section, directions through points are also generated randomly. Then both the image point positions and projected directions are perturbed with random noise. A subset of the points (30%) are chosen as outliers with large perturbations on both the positions and angles of the directions. We compare the solvers for two points and one 1-quiver ($P2Q1$) and one 1-quiver and one 2-quiver ($Q1Q2$) with the P4P solver in [4]. For each of the solvers, we choose the minimal set of data required for RANSAC, the distribution of the ratio of inliers of each RANSAC loop in shown in Figure 8. Here we define the inliers as the image points with reprojection errors less than a predefined threshold. It is not surprising to see that the $Q2Q1$ solver performs the best with respect to recovering inliers since it only requires two points. While ($P2Q1$) performs slightly worse, it still gives better results than the P4P solver which needs at least 4 point correspondences.

4.2. Real Data

We took 16 images of seven cardboards placed in a non-planar configuration with varying focal lengths (Figure 9), using a standard Canon EOS 50D camera. Each cardboard is attached with a pattern with dark and light squares for the ease of line detection. The automatic line detection algorithm detected 6 lines for each of the card board, and 9 points as the intersections of those lines. Thus, we have in total 63 points, 42 lines and 63 2-quivers.

We used these images to verify the applicability of the proposed solvers on real images with point, line and quiver features. The lines were estimated by sub-pixel edge-detection, cf. [2, 3]. This makes it possible to both estimate edge positions and edge position uncertainty. Lines as well as the uncertainty in their parameters were then obtained by fitting to these data. Finally points and their uncertainty

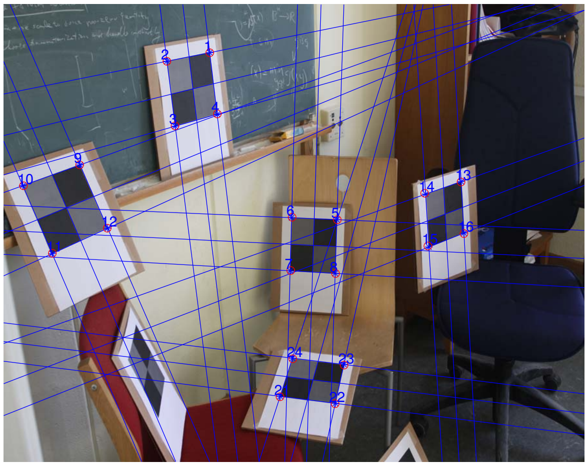

Figure 9. One of the Images of cardboards with detected lines and points.

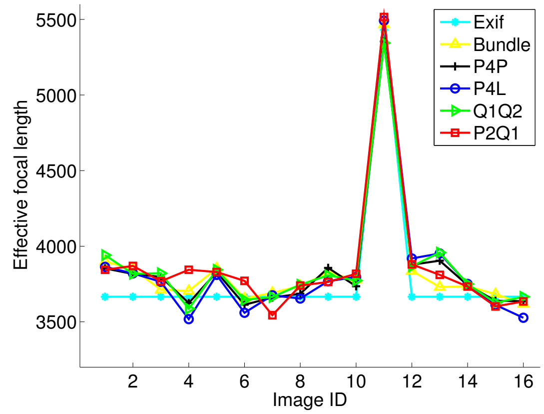

Figure 10. Statistics of focal length estimation of different solvers, bundle adjustment and exif-tag for the Cardboard dataset.

were estimated by intersection of two or more such lines. For 16 images, there are in total 621 visible measurements of the points (2-quivers) and 456 measurements of lines. The output is thus a number of image points, image lines, and image quivers as illustrated in Figure 1. Ground truth for 3D features were then obtained by bundle adjustment. In the bundle adjustment we used the estimated uncertainties in the image features.

The resulting construction of the 3D points and the camera poses as well as the focal lengths after bundle adjustment are fairly accurate and thus serves as ground truth. Given the reconstruction of the detected lines and intersection points, we use the proposed solvers to estimate both the camera poses and the focal lengths for each of the image. The estimations are then compared with the results given by the reconstruction. Due to the high quality of the reconstruction, the data can be seen as outlier-free. We first look at the reprojection errors of the poses and focal lengths estimated using different solvers and investigate whether the solvers adapt to real image noisy measurements. To measure the reprojection errors, we run different solvers in a RANSAC manner by choosing random minimal measurements. The average reprojection errors of image points for each solver are reported in Table 2. We can see from Table 2 that the errors of all our proposed solvers are similar to the $P4P$ solver.

	$P4P$	$P2Q1$	$Q1Q2$	$P4L$
Errors	2.463	2.531	3.123	3.141

Table 2. Average reprojection errors (in pixels) of image points with camera poses and focal lengths of the 16 images estimated with different solvers.

To further test the performance of the solvers, we also generate outliers by adding large synthetic perturbations to a random subset (30%) of image point positions, quiver directions and lines. We then run RANSAC (1000 runs for each image) on the perturbed data. For the inlier threshold of 3 pixels, the number of inliers (among in total 621 measurements) and the average reprojection errors for inliers are reported in Table 3. For this specific example, $P4P$ and $P2Q1$ output higher count of inliers and in the meantime has lower average reprojection errors. The slightly inferior performance of $Q1Q2$ and $P4L$ solvers might be due to the sensitivity of both solvers to measurement errors in the quiver directions and lines.

	$P4P$	$P2Q1$	$Q1Q2$	$P4L$
Inliers	309	298	253	223
Errors	1.502	1.330	1.402	1.633

Table 3. Number of inliers and average reprojection errors (in pixels) of inliers with 30% synthetic outliers for the cardboard dataset.

To evaluate the accuracy of the solvers, we compare the best focal length estimated (the one with maximum number of inliers) for each solver against the output from bundle adjustment as well as those extracted from EXIF-tag (conversion from 35mm film equivalent). We set the inlier threshold to be 2 pixels and run RANSAC on the original data without synthetic perturbation. The statistics of the estimated focal lengths are shown in Figure 10. It is noted that the focal lengths given by the exif information seems to be very coarse compared to those estimates from image data directly. We can also see that all solvers gives fairly similar estimates to the results from bundle adjustment.

5. Discussions

For the simpler calibrated pose estimation problem, we also see the potential of combining the simplicity the quaternion parameterization and the stability of Gröbner basis solvers. In [9], the minimal case of equivalently two 1-quivers (the direction is detected as the tangent to curves instead of arbitrary direction) for pose estimation was studied. A closed form solution for a polynomial equation of degree 16 was derived through rather involved calculation. With the quaternion formulation, we directly arrive at 3 quadratic equations on 3 unknowns $\{b, c, d\}$ (see supplementary materials) which is extremely fast to solve using Gröbner basis solver (approximately 1ms) compared to a few milliseconds of the released implementation for [9]. Though it is not fair to compare the time performance for unoptimized codes (both of them), it could still suggest superiority of the easy formulation and implementation of the Gröbner basis based solvers[1].

6. Conclusions

In this paper, we present several novel cases for pose estimation with unknown focal length utilizing combinations of points, lines and quivers. Here a quiver is an interest point with one or several directions attached to it. Pose for combinations of features allow for fewer feature correspondences and generate larger inlier sets with higher probability. Solving these new minimal cases is of both theoretical interests and practical importance. We have shown that these solvers are fast and numerically stable. This is verified in experiments with both synthetic and real data. The availability of such solvers will serve as an important step towards pose estimation with richer features and also shed light on structure from motion problem with line/direction features which are common in urban scenes.

As future work, it is of great theoretical importance to study the critical configurations for combinations of these features. The other key direction is to evaluate the application of new solvers to discriminative feature like SIFT to ease the correspondence problem for edges (direction of a quiver and line). One potential way is to make use of the dominant gradient directions given by SIFT and treat them as quiver directions. Then the correspondence problem is made relatively easier. In this case, one need to verify whether the solvers are robust against noisy estimation of the gradient directions. To improve the speed and numerical stability of the solvers, it is of interest to resolve the intrinsic symmetry in the quaternion parameterization either by algebraic manipulation or by deriving alternative set of constraints using geometric invariances.

Acknowledgement The research leading to these results has received funding from the strategic research projects ELLIIT and eSSENCE, Swedish Foundation for Strategic Research projects ENGROSS and VINST (grant no. RIT08-0043).

[1]Codes for the proposed solvers are available for download at http://www2.maths.lth.se/vision/downloads/.

References

[1] M. A. Abidi and T. Chandra. A new efficient and direct solution for pose estimation using quadrangular targets: Algorithm and evaluation. *Pattern Analysis and Machine Intelligence, IEEE Transactions on*, 17(5):534–538, 1995.

[2] K. Åström and A. Heyden. Stochastic modelling and analysis of sub-pixel edge detection. In *International Conference on Pattern Recognition*, 1996.

[3] K. Åström and A. Heyden. Stochastic analysis of scale-space smoothing. *Advances in Applied Probability*, 30(1), 1999.

[4] M. Bujnak, Z. Kukelova, and T. Pajdla. A general solution to the p4p problem for camera with unknown focal length. In *Proc. Conf. Computer Vision and Pattern Recognition, Anchorage, USA*, 2008.

[5] M. Bujnak, Z. Kukelova, and T. Pajdla. New efficient solution to the absolute pose problem for camera with unknown focal length and radial distortion. In *Computer Vision–ACCV 2010*, pages 11–24. Springer, 2011.

[6] M. Byröd, K. Josephson, and K. Åström. Fast and stable polynomial equation solving and its application to computer vision. *Int. Journal of Computer Vision*, 84(3):237–255, 2009.

[7] H. H. Chen. Pose determination from line-to-plane correspondences: existence condition and closed-form solutions. In *Computer Vision, 1990. Proceedings, Third International Conference on*, pages 374–378. IEEE, 1990.

[8] M. Dhome, M. Richetin, J.-T. Lapreste, and G. Rives. Determination of the attitude of 3d objects from a single perspective view. *Pattern Analysis and Machine Intelligence, IEEE Transactions on*, 11(12):1265–1278, 1989.

[9] R. Fabbri, B. Kimia, and P. Giblin. Camera pose estimation using first-order curve differential geometry. In *ECCV*, 2012.

[10] M. A. Fischler and R. C. Bolles. Random sample consensus: a paradigm for model fitting with applications to image analysis and automated cartography. *Communications of the ACM*, 24(6):381–95, 1981.

[11] D. Grayson and M. Stillman. Macaulay 2. Available at http://www.math.uiuc.edu/Macaulay2/, 1993-2002. An open source computer algebra software.

[12] R. M. Haralick, C. Lee, K. Ottenberg, and M. Nölle. Analysis and solutions for the three point perspective pose estimation problem. In *Proc. Conf. Computer Vision and Pattern Recognition*, pages 592–598, 1991.

[13] R. Hartley and H. Li. An efficient hidden variable approach to minimal-case camera motion estimation. *PAMI*, 2012.

[14] R. I. Hartley and A. Zisserman. *Multiple View Geometry in Computer Vision*. Cambridge University Press, 2000.

[15] J. A. Hesch and S. I. Roumeliotis. A direct least-squares (dls) method for pnp. In *International Conference on Computer Vision (ICCV)*, pages 383–390. IEEE, 2011.

[16] A. Irschara, C. Zach, J.-M. Frahm, and H. Bischof. From structure-from-motion point clouds to fast location recognition. In *Computer Vision and Pattern Recognition, 2009. CVPR 2009. IEEE Conference on*, pages 2599–2606. IEEE, 2009.

[17] B. Johansson, M. Oskarsson, and K. Åström. Structure and motion estimation from complex features in three views. In

Indian Conference on Computer Vision, Graphics and Image Processing, 2002.

[18] K. Josephson and M. Byröd. Pose estimation with radial distortion and unknown focal length. In *Proc. Conf. Computer Vision and Pattern Recognition, San Fransisco, USA*, 2009.

[19] K. Josephson, M. Byröd, F. Kahl, and K. Åström. Image-based localization using hybrid feature correspondences. In *The second international ISPRS workshop BenCOS 2007, Towards Benchmarking Automated Calibration, Orientation, and Surface Reconstruction from Images*, 2007.

[20] K. Köser and R. Koch. Differential spatial resection-pose estimation using a single local image feature. In *Computer Vision–ECCV 2008*, pages 312–325. Springer, 2008.

[21] Y. Kuang and K. Åström. Numerically stable optimization of polynomial solvers for minimal problems. In *Computer Vision–ECCV 2012*, pages 100–113. Springer, 2012.

[22] Z. Kukelova, M. Bujnak, and T. Pajdla. Automatic generator of minimal problem solvers. In *Proc. 10th European Conf. on Computer Vision, Marseille, France*, 2008.

[23] Z. Kukelova, M. Bujnak, and T. Pajdla. Polynomial eigenvalue solutions to the 5-pt and 6-pt relative pose problems. *BMVC 2008*, 2(5), 2008.

[24] V. Lepetit, F. Moreno-Noguer, and P. Fua. Epnp: An accurate o (n) solution to the pnp problem. *International Journal of Computer Vision*, 81(2):155–166, 2009.

[25] F. M. Mirzaei and S. I. Roumeliotis. Globally optimal pose estimation from line correspondences. In *Robotics and Automation (ICRA), 2011 IEEE International Conference on*, pages 5581–5588. IEEE, 2011.

[26] A. Penate-Sanchez, J. Andrade-Cetto, and F. Moreno-Noguer. Exhaustive linearization for robust camera pose and focal length estimation. 2013.

[27] S. Ramalingam, S. Bouaziz, and P. Sturm. Pose estimation using both points and lines for geo-localization. In *Robotics and Automation (ICRA), 2011 IEEE International Conference on*, pages 4716–4723. IEEE, 2011.

[28] B. Triggs. Camera pose and calibration from 4 or 5 known 3d points. In *Proc. 7th Int. Conf. on Computer Vision, Kerkyra, Greece*, pages 278–284. IEEE Computer Society Press, 1999.